

# Quantitative Mapping of Hydrodynamic Vegetation Density of Floodplain Forests Under Leaf-off Conditions Using Airborne Laser Scanning

Menno W. Straatsma

## Abstract

In this paper a method is presented to extract hydrodynamic vegetation density from airborne laser scanner data, relevant for exceedance levels of embankments of lowland areas. Two indices to predict vegetation density from the laser data were considered: (a) Percentage Index (PI) of points in the height interval inundated by the water, and (b) the Vegetation Area Index (VAI) that corrects for occlusion from the crown area. A computer simulation, using a digital forest model, showed a sensitivity of the indices for laser pulses that were sent out, but not detected by the laser receiver. The locations of these invalid points were therefore reconstructed. Two different assumptions were tested to assign new coordinates to these so-called invalid points. Percentage Index, with the invalid points reconstructed by means of thresholding the point density ratio, proved the best predictor ( $R^2 = 0.66$ ) of vegetation density of deciduous floodplain forests under winter conditions.

## Introduction

Hydrodynamic vegetation roughness, i.e., the retardance of water flow velocity by vegetation, is an important parameter to accurately model water levels and flow velocities of inundated floodplains (Darby, 1999; Tsujimoto, 1999; Stolker *et al.*, 1999; Huthoff and Augustijn, 2004). Forest is an important type of floodplain vegetation to be mapped accurately because its roughness is high and therefore strongly influences flood water levels. Moreover, forests grow in space and time in the case of natural succession, and the density can change rapidly, especially in young forests (Den Ouden, 1993). Various methods have been proposed to compute the roughness of forests. Petryk and Bosmajian (1975) and Pasche (1984) consider the stems as rigid cylinders and define the hydrodynamic vegetation density and stem drag as the requisite parameters. The hydrodynamic vegetation density ( $Dv$ ) is defined as the projected plant area ( $A$ ) in the direction of the water flow ( $F$ ) per volume of water in which the vegetation stands (Figure 1). Under the assumption of cylindrical vegetation elements, vegetation density equals the product

of number of stems per square meter and average stem diameter ( $m^2/m^3$ ).

Flowing water also has a dynamic effect on the roughness as the vegetation trails downstream due to fast flowing water, thus streamlining the leaves and branches of the vegetation, which reduces the roughness (Kouwen and Fathi-Moghadam, 2000; Copeland, 2000). Additional parameters that describe these dynamic effects are the tree height, the modulus of elasticity, and a parameter that describes all aspects of plant deformation as a result of increasing flow velocity. A roughness model that includes the latter parameters was proposed and tested by Kouwen and Fathi-Moghadam (2000) for coniferous trees. Vegetation parameters that describe the dynamic effects of bending or the drag coefficient seem unlikely to be extractable from remote sensing data. These parameters, therefore, need to be derived from a laboratory or the field. The relative importance of dynamic effects remains to be assessed for deciduous floodplain forest under leaf-off conditions. Klaassen *et al.* (1999), for example, found that bending of submerged vegetation of lowland floodplains under winter conditions did not significantly lower the vegetation height. Many roughness models use rigid cylinders as vegetation elements for which vegetation density is an important parameter (Schröder and Nuding, 1986; Mertens, 1989; Klopstra *et al.*, 1997; Darby, 1999; Van Velzen *et al.*, 2003; Helmiö, 2002; Baptist *et al.*, 2007).

Information on vegetation spatial patterns of floodplain vegetation density is essential as input for hydrodynamic flow models based on rigid cylinders. Airborne and spaceborne remote sensing have become well-proven surveying techniques that provide primary information for vegetation classification over various different scales (Mertes, 2002). Satellite imagery was used to map floodplain vegetation at a regional scale (Ringrose *et al.*, 1988; Mertes *et al.*, 1995; Townsend and Walsh, 2001; Van der Sande *et al.*, 2003), while airborne multispectral images were used for kilometer-scale vegetation classification (e.g., Cusack *et al.*, 1999). In the Netherlands, the Ministry of Public Works, Transport and Water Management maps vegetation density based on

Photogrammetric Engineering & Remote Sensing  
Vol. 74, No. 8, August 2008, pp. 987–998

Department of Physical Geography, Faculty of Geosciences,  
Utrecht University, The Netherlands, PO Box 80115, 3508  
TC Utrecht (m.straatsma@geo.uu.nl).

0099-1112/08/7408-0987/\$3.00/0  
© 2008 American Society for Photogrammetry  
and Remote Sensing

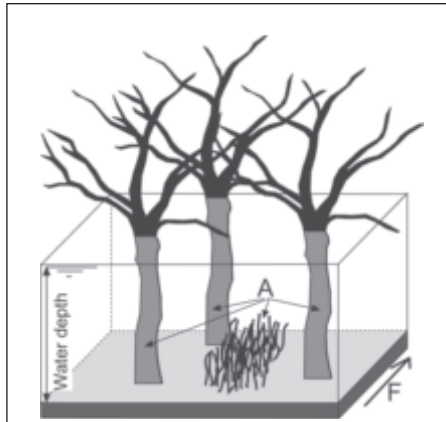


Figure 1. Sketch of hydrodynamic vegetation density ( $D_v$ ); the projected plant area, A, in the direction of the flow, F, per unit volume ( $m^2/m^3$ ).

so-called floodplain ecotopes. Ecotopes are “spatial landscape units that are homogeneous as to vegetation structure, succession stage and the main abiotic factors that are relevant to plant growth” (Leuven *et al.*, 2002). Nevertheless, Ritzen and Straatsma (2002) showed differences in vegetation density within single ecotopes of an order of magnitude. Ecotopes are delineated by manual classification of false color aerial photographs using an interpretation key (Jansen and Backx, 1998). These classified images or ecotope maps can subsequently be converted to vegetation density maps using a lookup table. The disadvantage of lookup tables is that within-unit spatial variability in vegetation density is not considered.

Airborne laser scanning (ALS) has become a tool for the automatic extraction of various forest structural characteristics related to vegetation density: stem number, stem

diameter, basal area, and/or timber volume (Lefsky *et al.*, 1999a; Lefsky *et al.*, 1999b; Means *et al.*, 1999; Næsset, 1997; Næsset and Bjercknes, 2001; Nilsson, 1996; Drake *et al.*, 2002; Næsset, 2002; Holmgren and Jonsson, 2004). Asselman (2002) related vegetation density at breast height to canopy statistics, which does not consider undergrowth. Floodwaters will typically inundate the floodplain forest to a depth of three meters. Airborne laser scanning, contrary to spectral remote sensing, is well able to penetrate into the forest canopy and detect the forest floor (Baltsavias, 1999a), and is therefore also expected to directly supply information about the vegetation density up to three meters above the forest floor. Recent attempts have been reported of floodplain roughness parameterization using vegetation heights from ALS data (Cobby *et al.*, 2001; Cobby *et al.*, 2003; Mason *et al.*, 2003; Hopkinson *et al.*, 2005). They do not include vegetation density in their roughness model. Currently, no method is available to account for the within-unit variation of hydrodynamic vegetation density of floodplain forest. The objective of this study was to assess the predictive quality of ALS for the quantitative mapping of hydrodynamic vegetation density of deciduous lowland floodplain forest with undergrowth under leaf-off conditions in the inundation height interval.

The study was carried out in three floodplain sections along the lower Rhine River during low flow. Field reference data of forest vegetation density were collected and compared to (a) the ecotope approach, and (b) laser-derived parameters. Special attention was paid to the laser pulses that were emitted, but whose reflection could not be detected.

## Materials and Methods

### Study Area

This study is based on laser data collected in three floodplain sections of the distributaries sections of the River Rhine in The Netherlands: “Duursche Waarden” floodplain (DW) along the right bank of the River IJssel, the “Afferden en Deestse Waarden” (ADW), and the “Gamerense Waarden” (GW) floodplains along the left bank of the River Waal (Figure 2).

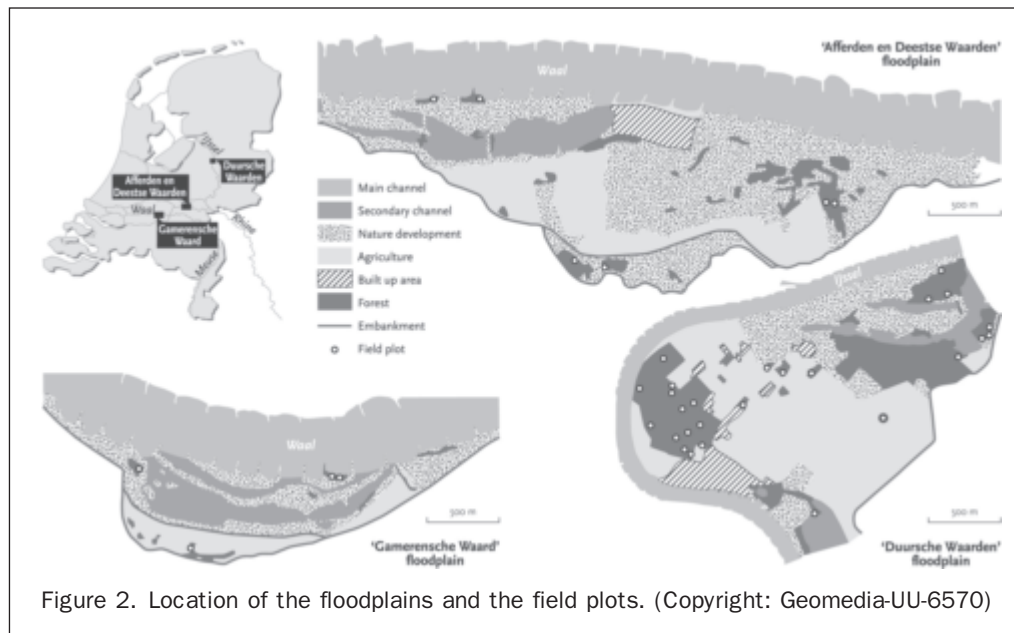


Figure 2. Location of the floodplains and the field plots. (Copyright: Geomedica-UU-6570)

In these floodplains, the Ministry of Public Works, Transport, and Water Management has been taking measures to reduce flood levels and simultaneously restore the ecology by means of digging side channels and extensive grazing by cattle (Nienhuis and Leuven, 2001; Van Stokkom *et al.*, 2005). The ministry also acquired high-density laser data as monitoring pilots. All floodplains are flat, and elevation differences are less than one meter except for the Duursche Waarden floodplain that contains a few wind-blown ridges of approximately 4 m high. Land-cover is a combination of arable land, meadows, open water, and nature areas that partly consist of forests. Forests comprise softwood forest (willow (*Salix alba*, *Salix viminalis*), poplar (*Populus nigra*, and *Populus x canadensis*)), hardwood forest (oak (*Quercus robur*), ash (*Fraxinus excelsior*)) in various stages of development, and a small mature pine stand (*Pinus sylvestris*). Forest coverage summed up to 22, 8, and 4 percent of the floodplain surface for the DW, ADW and GW floodplain, respectively, according to the ecotope map. All vegetation was in winter condition when the laser data was acquired. The typical inundation depth of these forests is 3 m, but it might rise to 5 m in the case of extreme flood events.

### Data Collection

#### Ecotope Maps

Ecotope maps are available for the whole embanked floodplain area in the Netherlands. They are based on visual interpretation of aerial photographs of 1996, scale 1:10 000 (Jansen and Backx, 1998). The smallest detected object was 20 m by 20 m in the field, or 2 mm by 2 mm on the aerial photo; hence, any variability at smaller scales is excluded from the map. Each forest ecotope is subsequently labeled with a vegetation density value using a lookup table (Van Velzen *et al.* 2003), based on limited field inventories in the Dutch floodplains. This results in a choropleth map with vegetation density values for the vegetated parts of the floodplain.

#### Field Measurements

Hydrodynamic vegetation density for forests ( $Dv$ ) was measured in the field at breast height (1.5 m above the ground) simultaneously with the laser scanning survey. In total, 36 plots were outlined in the field distributed over the three different floodplains. Plot size was at least 200 m<sup>2</sup> and varied according to tree size to ensure that at least 30 trees were inside the plot area. Georeferencing of the plots was done using a Garmin 12 handheld GPS system. In case the estimated point error (EPE), as given by the proprietary Garmin software, was more than 15 m; the positioning was done using the ecotope map. In each plot, the number of stems or shoots per m<sup>2</sup> ( $N$ ) were counted that cross a virtual horizontal plane, and the diameters of the stems were measured manually following Brown (1971). The average diameter ( $d$ ) was computed from 30 randomly selected stems, which included understory vegetation. Vegetation density ( $Dv$ ) was then computed as the product of  $N$  and  $d$ . Table 1 shows a summary of the field data.

TABLE 1. SUMMARY OF SAMPLE PLOT FIELD DATA. NUMBER OF FIELD PLOTS WAS 45 WITH AT LEAST 30 TREES PER PLOT

Characteristic	Range	Mean
$N$ (m <sup>-2</sup> )	2.1*10 <sup>-2</sup> -20	0.048
$d$ (m)	1.1*10 <sup>-2</sup> -0.46	0.11
$Dv$ (m <sup>2</sup> /m <sup>-3</sup> )	6.2*10 <sup>-3</sup> -0.24	0.049

$N$  = Number of stems per m<sup>2</sup>,  $d$  = diameter of stem at breast height (1.5 m),  $Dv$  = hydrodynamic vegetation density

#### Airborne Laser Scanning Data

The laser data were acquired using the FLI-MAP system mounted on a helicopter (Huising and Gomes-Pereira, 1998; Baltsavias, 1999b). FLI-MAP (Fast Laser Imaging and Mapping Airborne Platform) is a small-footprint, first pulse, scanning laser range finder combined with a DGPS and an Inertial Navigation System for positioning. An overview of the laser scanning technique used is given by Wehr and Lohr (1999). Table 2 summarizes the characteristics of the two laser scanning campaigns, and the locations are shown in Figure 2. The laser data collected in 2001 in the Duursche Waarden floodplain and the Afferdensche en Deestse Waarden floodplain was collected with a single, nadir looking laser scanner, which resulted in the DW-ADW dataset. Between 2001 and 2003, Fugro-Inpark added a second laser range finder to FLI-MAP, resulting in a doubling of the data collection rate and a re-orientation of the scanners. Instead of one nadir looking scanner, the two scanners were facing 7° forward and backwards to decrease the number of occlusions in built-up areas. With the new FLI-MAP configuration, the dataset was collected in the Gamerense Waard floodplain in 2003 (GW dataset). For this pilot study, each of the flight lines of the Gameren floodplain was flown twice, to increase the point density even further.

Usual FLI-MAP data products consist of the X-Y-Z of the laser hits in a local coordinate system combined with the optional reflection intensity. Moreover, points are exported only if a significant return is detected by the receiver of the laser range finder. These points will be referred to as *valid* since their coordinates were computed using a valid range value. Points that were emitted, but did not give a significant return were included in the raw data set as well. The low reflection intensity could result from absorption or specular reflection at the object. Hardware-related reasons for a low reflection intensity include an old laser diode or a mal-calibration of the focus of the laser receiver, which amplifies the return signal. According to the laser data vendor, the laser range finder is calibrated during each change of laser diode. Mal-calibration of the receiver would lead to such a reduction in return intensity such that it precludes laser surveying, whereas an aging diode would give a small overall reduction in intensity. No distinction between the two potential error sources could be made from the laser point cloud. A default range value of 300 m was assigned to the pulses without a valid range measurement. These points will be referred to as *invalid* points. Both valid and invalid points were included

TABLE 2. METADATA FOR THE TWO LASER SCANNING CAMPAIGNS

Acquisition Time	Floodplain Location <sup>a</sup>	Scan Angle	Scan Line Orientation	No. of Sensors	Pulse Rate	Flying Height	Point Density	Flight Lines <sup>b</sup>
March 2001	DW-ADW	±30°	Nadir	1	10 kHz	80 m	12 m <sup>-2</sup>	Single
March 2003	GW	±30°	±7°	2	2*10 kHz	80 m	75 m <sup>-2</sup>	Double

<sup>a</sup>DW = Duursche Waarden, ADW = Afferden en Deestse Waarden, GW = Gamerense Waard

<sup>b</sup>For the GW dataset, each flight line was flown two times to increase the point density.

in the raw datasets. Point validity and time of firing of the laser pulse were added as attributes. In a separate file, the positions of the laser scanner were given, which also had a time stamp. The two time stamps were used in subsequent data processing. Temporal frequency of the scanner position output was 50 Hz. Figure 3 shows the scanner positions, and valid/invalid data of one flight strip.

### Indicators for Vegetation Density

#### Ecotopes and Lookup Table

To assess the predictive quality of the method based on ecotope maps, the ecotope type was taken from the ecotope map, and the vegetation density was taken from the lookup table presented in (Van Velzen *et al.*, 2003). The field reference data were compared to values from the lookup table. The predictive quality of the ecotope approach served as a reference for vegetation density prediction derived from airborne laser scanning.

#### Laser-derived Parameters

##### DTM Processing

Before vegetation indices could be computed, the effect of the topography had to be eliminated by creating a Digital Terrain Model (DTM) for each plot. The first step in the laser data processing was the selection of the points located within the plots laid out in the field. Other laser points were not taken into account for this study. A DTM was constructed using iterative residual analyses based on a simplified version of the method of Kraus and Pfeifer (1998). In each step, a surface was computed as the local average in a moving window. The window radius was 2 m; a larger window would lead to a loss of detail and a smaller window would lead to an erroneous DTM, as in some cases no ground points occurred within the window. The residual distance to this surface was computed for each point. Points with positive residuals are likely to be vegetation points. The range of values for a non-vegetated, flat surface was

computed and proved approximately 15 cm above and below average, comparable to Davenport *et al.* (2000). Therefore, points with a residual value of more than 15 cm were excluded from further analyses in the DTM processing. With the remaining points, iterations were continued until all residuals were less than 15 cm. Heights relative to the DTM were used in subsequent computations.

##### Percentage Index

Vegetation density was predicted from ALS data by two indices. The percentage index (*PI*) computes the percentage of laser hits that fall within the height range (*h1* to *h2*) that could be inundated by the water:

$$PI_{h1-h2} = \frac{1}{h2 - h1} \cdot \frac{N_{h1-h2}}{N_{tot}} \quad (1)$$

in which  $N_{h1-h2}$  is the number of points between height 1 and 2 above the forest floor, and  $N_{tot}$  is the total number of points in the field plot including canopy and ground surface points. The height interval for *PI* was set to 0.5 to 2.5 m, the region around breast height where the vegetation density was measured in the field, to optimize the representation of the laser data. The distance between *h1* and *h2* should not be too small, otherwise too few points would be present within the height interval of interest. Moreover, *h1* was set to 0.5 m to remain well above the noise height of the ground surface points. This method does not take occlusion from the crown area into account. Tree crowns reflect part of the laser pulses, thereby reducing the number of points available for detection of stems or the ground surface. However, the crown density is small (25 percent) under leaf-off conditions.

##### Vegetation Area Index

The optical point quadrat method, introduced by MacArthur and Horn (1969), compensates for occlusion. Later, it was verified by Aber (1979). This method calculates a Leaf Area

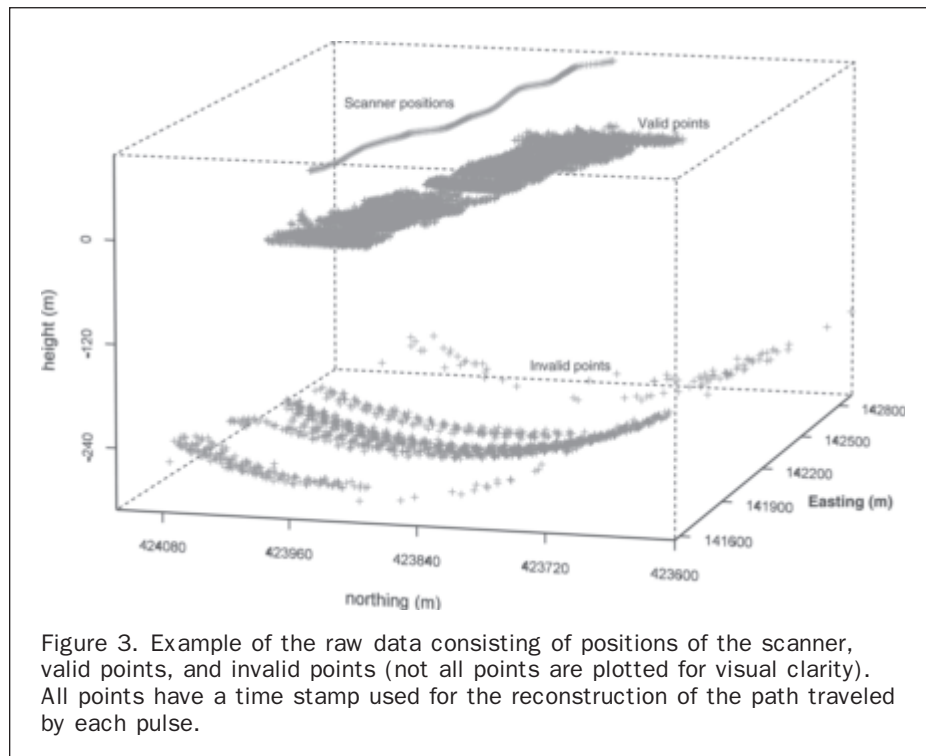


Figure 3. Example of the raw data consisting of positions of the scanner, valid points, and invalid points (not all points are plotted for visual clarity). All points have a time stamp used for the reconstruction of the path traveled by each pulse.

Index for specific height increments, in a similar way as the extinction of light in a semi-transparent medium. Recently, Lefsky *et al.* (1999a) successfully modified the MacArthur-Horn method to generate canopy height profiles. Canopy height profiles not only include foliage, but also woody vegetation. The forests considered in the present study were all leafless. The assumption was made that the mechanism of occlusion from trees in leaf-off condition is similar to occlusion from trees in leaf-on conditions. Laser hits are in this case intercepted by branches instead of leaves. The resulting value is therefore not a *Leaf Area Index*, but a woody *Vegetation Area Index (VAI)*. Like *PI*, the *VAI* is computed only over the height interval that is inundated by the water using the following equation:

$$VAI_{h_1-h_2} = \frac{1}{h_2 - h_1} \cdot \ln\left(\frac{N_{h_2}}{N_{h_1}}\right) \quad (2)$$

in which  $N_{h_1}$  and  $N_{h_2}$  are the number of points below heights  $h_1$  and  $h_2$  ( $h_2 > h_1$ ), which includes ground points. The first term in the formula is introduced to make the *VAI* independent of the height interval. However, four assumptions underlie this method: (a) all laser pulses enter the forest with an equal incidence angle, (b) no clumping is present, which means that the horizontal distribution of vegetation elements is random (Jonckheere, 2004), (c) all vegetation elements have an equal angle with a horizontal plain, and (d) all elements have an equal probability of detection, which means an equal reflectivity. Strictly speaking, none of these assumptions is fulfilled in the case of floodplain forest and airborne laser scanning observation.

#### Simulation Experiments

To analyze the effects of different laser settings and vegetation densities on *PI* and *VAI*, a computer simulation was carried out using a simplified forest-canopy scheme. The forest scheme consisted of a digital forest model and a ground surface. Trees had a stratified random spatial arrangement and were represented as a beam-shaped stem and a disc-shaped horizontal crown. A full 3D tree-branch model was outside the scope of this paper. The crown was simplified to a simple disc, since it is above the inundation height. To mimic the amount of occlusion of real a floodplain forest in winter (25 percent at 15 m), the crown radius was set to 1.25 m at a tree spacing of 5 m. The crowns were not transparent, which comes close to first pulse characteristics since only 25 percent of the pulses are occluded by the canopy. Tree height was set to 15 m. The ground surface was horizontal. The laser pulse configuration was based on laser scanning settings similar to *FLI-MAP*; flying height was set to 80 m and the lateral scan angle to  $\pm 30^\circ$ . The point density was variable. The simulation computes the coordinates of intersection between the *trees* and simulated laser pulses (Figure 4).

For each simulation, the vegetation density was computed from the stem spacing and thickness. *PI* and *VAI* were computed from the resulting point cloud. The following effects were evaluated quantitatively:

- The relation between vegetation density and *PI* and *VAI*. Using one laser point per  $m^2$ , vegetation density was varied stepwise between 0.003 to 0.2  $m^2/m^3$ .
- The minimum number of laser points needed in the *VAI* interval (0.5–2.5 m) for a robust *VAI* estimation. Due to the random effect in the tree distribution, the resulting *PI* and *VAI* values varied between individual simulations for the same forest setting. Therefore, a suite of simulations was carried out in which point densities were decreased stepwise from four points per  $m^2$  to one point per 400  $m^2$ . For each point density, 30 simulations were run, which enabled the

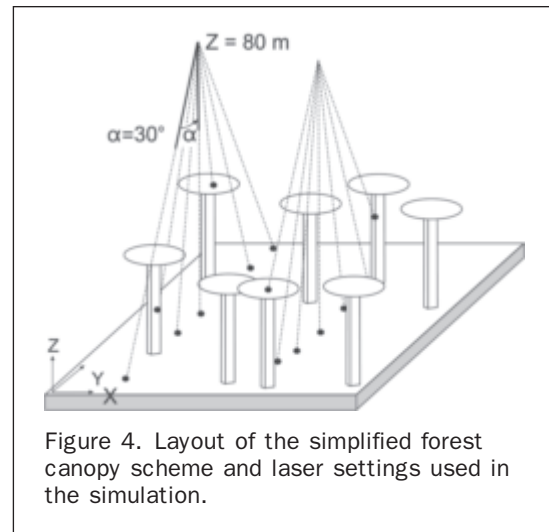


Figure 4. Layout of the simplified forest canopy scheme and laser settings used in the simulation.

computation of the coefficient of variation as a function of number of points in the height interval  $h_1$  to  $h_2$ .

- The effect of the number of ground points on the *VAI* and *PI* value, allowing for determining the effect of loss of returns from the ground surface.
- The effect of increasing the incidence angle on *VAI* and *PI*.

The incidence angle of the pulse, the angle between nadir and the firing direction, varies over the width of the scan strip. At nadir, a laser pulse will never hit a vertical stem, while along the edges, the probability of hitting a stem proportionally increases due to the longer trajectory through the vegetation and the larger angle between the stem and the laser pulse, which also resulted from a simulation by Holmgren *et al.* (2003) for canopies. Contrary to the true scan pattern where the scan angle varied over the width of the scan strip, laser pulses in these simulations were generated with equal incidence angles over the whole plot. The incidence angle was, therefore, varied stepwise from  $0^\circ$  to  $40^\circ$  in  $2^\circ$  increments. The upper limit of  $40^\circ$  represents the combination of the scan line orientation ( $\pm 7^\circ$ ), scan direction ( $\pm 30^\circ$ ), and movement of the helicopter.

#### *PI* and *VAI* Computation Using Invalid Points

Both *PI* and *VAI* relate the density of laser points in the inundation height to vegetation density, and assume equal probability of detection for vegetation and ground surface. However, up to 53 percent of the emitted laser pulses was not detected by the laser receiver due to: (a) low reflectance of the ground surface combined with (b) mirroring away of the laser energy at large scan angles, (c) trapping of the reflected pulse in the tree crown, (d) an old laser diode, or (e) miscalibration of the laser receiver. In some cases, large numbers of pulses got absorbed by the ground surface. For example, the spatial distribution of valid ground points showed a stripy pattern in one of the field plots, related to the presence of ditches. The loss of returns could influence *PI* as it affects the number of points within the inundation height or the total number of points ( $N_{h_1-h_2}$ , and  $N_{tot}$ ; Equation 1), and influences *VAI* through the number of points below height 1 and height 2 ( $N_{h_1}$ , and  $N_{h_2}$ ; Equation 2). Given the large number of invalid returns, they needed to be incorporated in the computation of *PI* and *VAI*, which consisted of three steps for each plot.

The first step consisted of selecting those invalid points that were absorbed inside the plot areas. To that end, points were reconstructed to ground height. For each plot, all

invalid points were selected within a buffer around the boundaries of the field plot. Figure 5a illustrates this with a view in the flight direction. The width for the buffer is determined by the flying height and the scan angle, and was set to 150 m outside the plan-view boundaries of the plot. The timestamps were used to locate the scanner position for each invalid point. The scanner position and the point position give two points of the path that the pulse would have traveled in the absence of a ground surface. To determine whether a pulse indeed passed through the plot, its X-Y coordinates at the height of the ground surface were determined. The surface elevation of the valid point that is closest *in time* with the invalid point was used as the Z coordinate for each invalid point (Figure 5b). The X-Y coordinates of the invalid points were found by intersecting the line between point and scanner position with a plane at height Z. As a result, the new position of the invalid points is located on the line that the laser pulse has traveled. Only points whose reconstructed X-Y values were inside the plot boundary were used in further analyses.

The second step consisted of determining which points were absorbed at the ground surface. Two assumptions were tested. The first assumed that the ground surface absorbed the energy of all invalid points. In this case, X-Y-Z coordinates of the invalid point were assigned using the same method as in the previous step. Figure 5b shows the location of the reconstructed point using the first assumption. Visual inspection showed that in a few plots a spatial pattern existed due to the presence of water, for example, in ditches or lower areas of the plot. In other plots however, such a pattern was neither visible in the data, nor in the field. The second assumption, therefore, was that the energy got absorbed in the vegetation layer or at the ground surface. To make the distinction between points that got lost by absorption on the ground or within the vegetation layer, the Point Density Ratio (*PDR*) was defined:

$$PDR = \frac{N_{local\_invalid}}{N_{local\_valid}} \quad (3)$$

where  $N_{local\_invalid}$  is the local point density of the invalid points reconstructed to the ground level.  $N_{local\_valid}$  refers to the local point density of all valid points. Both were computed in a local neighborhood using a moving window with a 0.5 m radius to maintain spatial detail in point density differences. When the *PDR* is high, relatively many points in a local neighborhood were absorbed, indicating that a low reflective ground surface was present, which is likely due to water on the ground surface. Points with a higher ratio were therefore assumed absorbed on the ground. Conversely, points with a low *PDR* do not have a specific height of absorption. A range of *PDR* values was tested as a threshold, and a *PDR* of 0.7 gave the best prediction results. Invalid points with a *PDR* higher than 0.7 were selected, and their height set to the DTM height of the temporal most proximal point. Invalid points with a *PDR* less than 0.7 were excluded from further analyses.

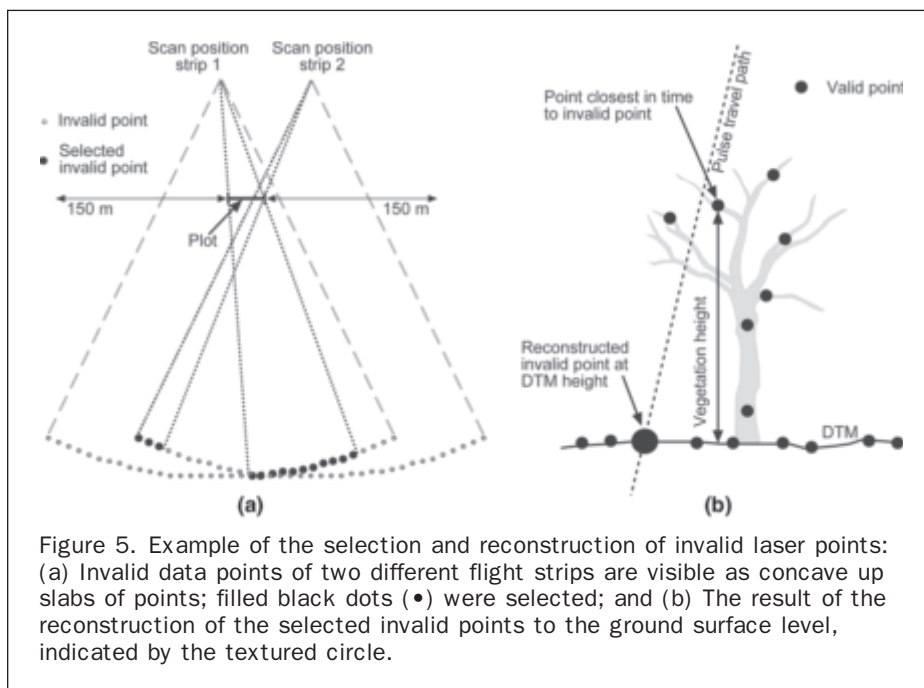
In the final step, *PI* and *VAI* values were computed for the three different point distributions: (a) valid points only ( $PI_{valid}$ ,  $VAI_{valid}$ ), (b) valid points plus all invalid points reconstructed to the ground surface ( $PI_{inv.grd}$ ,  $VAI_{inv.grd}$ ), and (c) valid points plus invalid points set to ground level in case the point density ratio was more than 0.7 ( $PI_{inv.PDR}$ ,  $VAI_{inv.PDR}$ ).

#### Incidence Angle and Reflection Intensity

The time stamp on the scanner positions and the point position facilitated the computation of the incidence angle ( $\alpha$ ) for each point. The incidence angle was computed by:

$$\alpha = \arccos\left(\frac{\sqrt{(dz)^2}}{\sqrt{(dx)^2 + (dy)^2 + (dz)^2}}\right) \quad (4)$$

where  $dx$ ,  $dy$ , and  $dz$  are the differences in X, Y, and Z coordinates between scanner and point position in the raw data. The average incidence angle per plot was computed for the hits between  $h1$  and  $h2$ . Additionally, the reflection intensity as registered by the laser scanner was averaged for the valid points between  $h1$  and  $h2$ .



## Vegetation Density Prediction

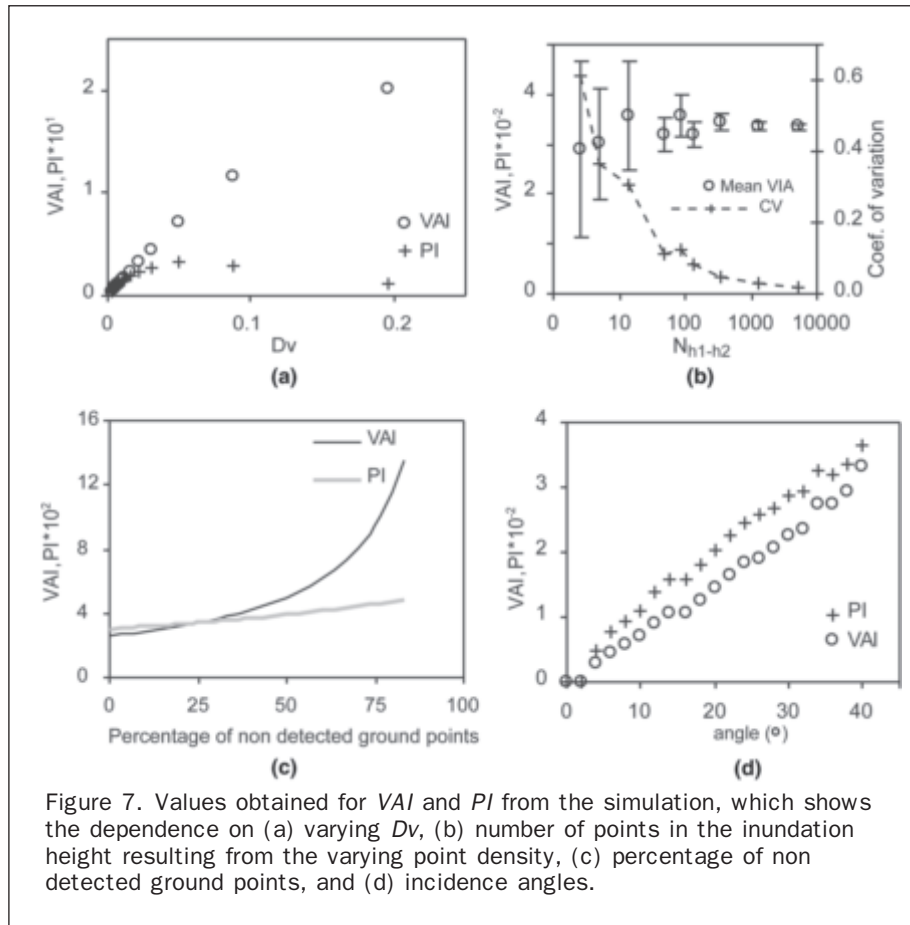
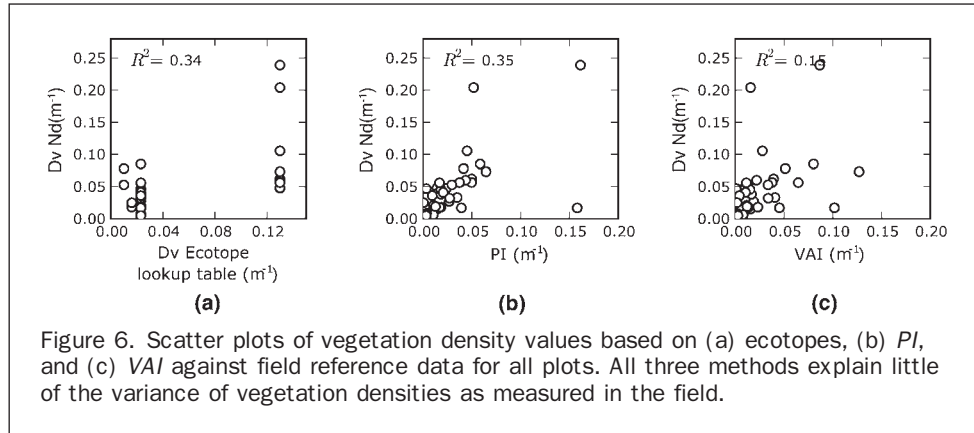
### Estimates for All Field Plots

Figure 6 shows the scatter plots between the 36 observed vegetation densities ( $Dv$ ) in the field and (a) ecotope approach prediction of  $Dv$ , (b) the percentage index ( $PI$ ) of laser points in the inundation height, and (c) the Vegetation Area Index. Regression analyses showed that all methods explain only a small part of the variance in vegetation density as measured in the field. The ecotope prediction shows four classes. The vertical range per cluster indicates the range of vegetation densities that occur within each ecotope type.  $PI$  and  $VAI$  show a linear relation close to the origin, but large outliers are present that underestimate or

overestimate the vegetation density. The ecotope approach ( $R^2 = 0.34$ , residual standard error (RSE) = 0.040) performs equally well as the  $PI$  ( $R^2 = 0.35$ , 0.040), but better than the  $VAI$  ( $R^2 = 0.15$ , RSE = 0.046).

### Simulation Results

The simulation provided insight in the sensitivity of the vegetation density indices to the four effects mentioned in *Simulation Experiments* section. Figure 7a shows that  $PI$  increases from 0 up to vegetation densities of  $0.06 \text{ m}^2/\text{m}^3$  and then decreases.  $VAI$  increases linearly with  $Dv$  over the range of vegetation densities from  $0.003$  to  $0.2 \text{ m}^2/\text{m}^3$ . For vegetation densities up to  $0.04 \text{ m}^2/\text{m}^3$ , the curves for  $PI$  and  $VAI$  are similar.



The influence of the number of points in the height interval ( $N_{h_1-h_2}$ ) on the determination of  $VAI$  is shown in Figure 7b. The error bars indicate the standard deviation of the  $VAI$  of the 30 simulations. With increasing number of points, the standard deviation and coefficient of variation decrease as expected. A coefficient of variation (cv) of 0.15 was arbitrarily selected as a minimum acceptable level, which relates to 50 points for  $N_{h_1-h_2}$ . If the percentage of non-detected ground hits increases, both  $PI$  and  $VAI$  become higher (Figure 7c). This implies that if ground returns remain undetected,  $VAI$  and  $PI$  will be overestimated, (Equations 1 and 2).  $VAI$  is more sensitive to a loss of ground returns, indicated by the steeper slope of  $VAI$ .

Figure 7d shows the dependence of the  $PI$  and  $VAI$  on incidence angle. At a vegetation density representative for a normal forest ( $Dv = 0.022 \text{ m}^2/\text{m}^3$ ),  $PI$  and  $VAI$  both increase linearly over the  $0^\circ$  to  $40^\circ$  range. Similar results were found using other vegetation densities.

The simulation showed that large errors can be introduced in the estimation of  $PI$  and  $VAI$  due to (a) a low number of vegetation hits in the height range between  $h_1$  and  $h_2$ , and (b) when a large number of ground points are not detected. These effects have to be taken into account when  $PI$  or  $VAI$  are used to predict the hydrodynamic vegetation density.

#### Estimates for Selected Plots

Based on the simulation results (Figure 7b), only those plots that included more than 50 points in the inundation height were considered, which corresponds to a coefficient of variation of 0.15. Twenty-two plots satisfied the above condition. For this subset, the ecotope approach performed slightly worse than for all plots ( $R^2 = 0.28$ ,  $RSE = 0.024$ ; Table 3). Figure 8a shows a 3D scatter plot of a point distribution in case all invalid points are assigned a ground surface height. The stripy pattern of invalid points is related to the presence of ditches in this plot. The number of selected invalid points has a large influence on the vertical point distribution (Figure 8b).

Scatter plots of the relation between field values of vegetation density against  $PI$  and  $VAI$  are shown in Figure 9. The two left panels show  $PI_{valid}$  and  $VAI_{valid}$ , based on valid

points only. The middle two panels show the results in case all invalid points are assigned a ground height ( $PI_{inv.grd}$ ,  $VAI_{inv.grd}$ ).  $PI_{inv.grd}$  and  $VAI_{inv.grd}$  estimates are lower than  $PI_{valid}$  and  $VAI_{valid}$ , most notably for the DW-ADW plots. The two panels on the right show  $PI$  and  $VAI$  under the assumption that only invalid points with a  $PDR$  larger than 0.7 are ground points ( $PI_{inv.PDR}$  and  $VAI_{inv.PDR}$ ).  $PI$  proved a better predictor of vegetation density than  $VAI$ , even though  $PI$  does not correct for occlusion from the canopy. This was the case both before and after the correction using invalid points. Explained variance of  $PI$  varied between 0.55 to 0.66 when corrections for missed ground points were made compared to 0.27 and 0.36 for  $VAI$  (Table 3). Multiple regression models, using the average incidence angle per plot or intensity as additional parameters did not improve prediction.

Intensity values for the points in the inundation height ranged from 26 to 46 on a 0 to 255 scale for the DW-ADW dataset, and between 71 and 104 for the GW dataset. The difference in intensity values between the two datasets is significant at the 99 percent confidence level. No significant difference in means existed between the average incidence angles between the two datasets. The percentage of invalid points also differs significantly between the two datasets. The number of invalid points varied between 9 and 53 percent for the DW-ADW dataset and between 0.01, and 1.1 percent for the GW dataset. It is unlikely that this results from the upgrade of the FLI-MAP system between 2001 and 2003, because both systems were regularly calibrated. Partly, the difference results from the presence of water on the ground in the DW-ADW floodplains, either in the form of puddles or ditches. However, even dry plots showed a minimum of 9 percent invalid data points. The plots in the Garenen floodplain (GW) were all dry at the time of laser data acquisition. The large number of invalid points in the DW-ADW plots explains the sensitivity of these plots to the different estimates of  $PI$  and  $VAI$  (Figure 9).

#### Discussion

In this paper, field reference data are compared to three vegetation density mapping methods: ecotopes,  $PI$ , and  $VAI$ . Hydrodynamic vegetation density, as considered in

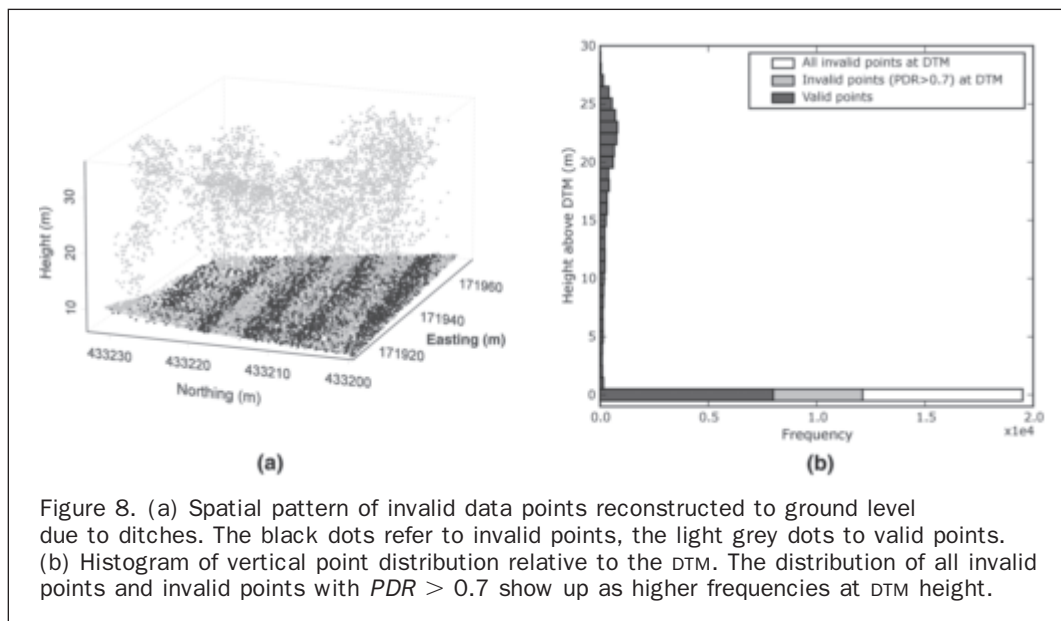


Figure 8. (a) Spatial pattern of invalid data points reconstructed to ground level due to ditches. The black dots refer to invalid points, the light grey dots to valid points. (b) Histogram of vertical point distribution relative to the DTM. The distribution of all invalid points and invalid points with  $PDR > 0.7$  show up as higher frequencies at DTM height.

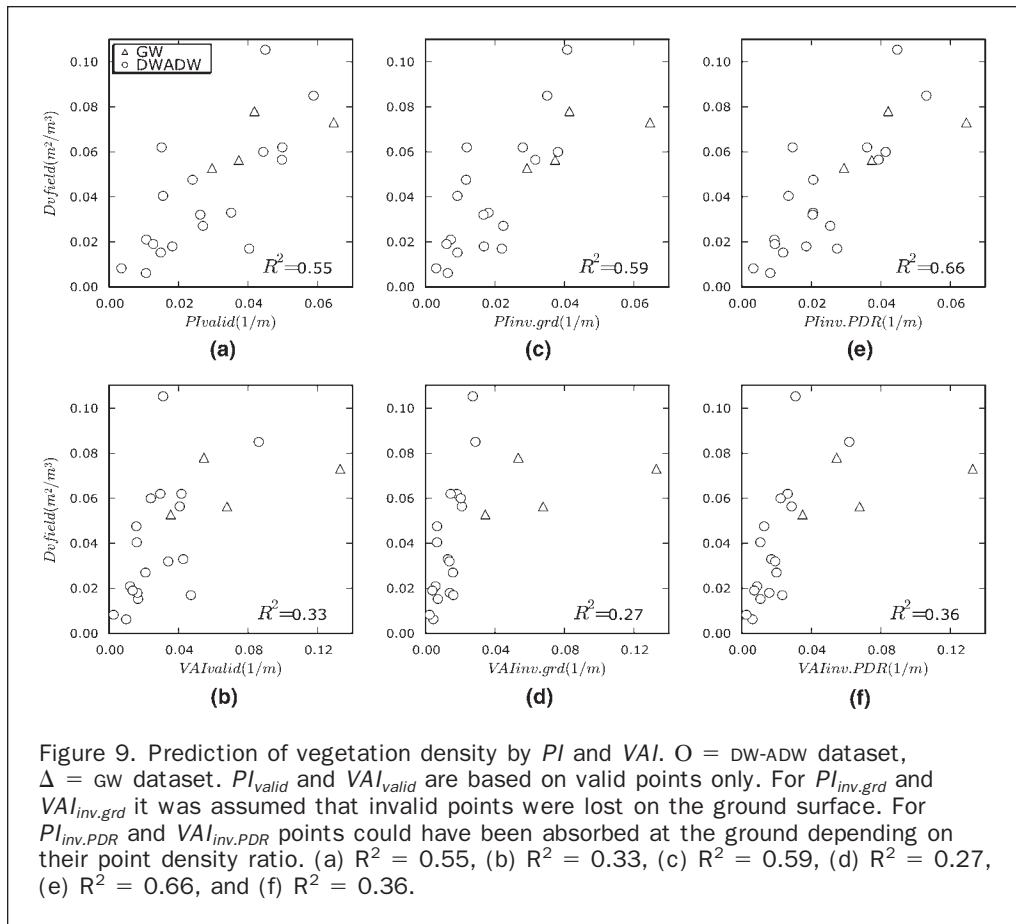


Figure 9. Prediction of vegetation density by  $PI$  and  $VAI$ .  $O$  = DW-ADW dataset,  $\Delta$  = gw dataset.  $PI_{valid}$  and  $VAI_{valid}$  are based on valid points only. For  $PI_{inv.grd}$  and  $VAI_{inv.grd}$  it was assumed that invalid points were lost on the ground surface. For  $PI_{inv.PDR}$  and  $VAI_{inv.PDR}$  points could have been absorbed at the ground depending on their point density ratio. (a)  $R^2 = 0.55$ , (b)  $R^2 = 0.33$ , (c)  $R^2 = 0.59$ , (d)  $R^2 = 0.27$ , (e)  $R^2 = 0.66$ , and (f)  $R^2 = 0.36$ .

TABLE 3. REGRESSION RESULTS FOR VEGETATION DENSITY PREDICTION

Regression Equation ( $N = 22$ )	$R^2$	RSE <sup>a</sup>
$Dv = 0.27 \cdot Dvecotopes + 0.029$	0.28	0.024
$Dv = 1.18 \cdot PI_{valid} + 0.008$	0.58	0.019
$Dv = 1.33 \cdot PI_{inv.grd} + 0.01$	0.59	0.018
$Dv = 1.36 \cdot PI_{inv.PDR} + 0.008$	0.66	0.016
$Dv = 0.53 \cdot VAI_{valid} + 0.03$	0.33	0.023
$Dv = 0.48 \cdot VAI_{inv.grd} + 0.03$	0.27	0.022
$Dv = 0.56 \cdot VAI_{inv.PDR} + 0.03$	0.36	0.022

<sup>a</sup>RSE = Residual standard error

this study, is a parameter that describes the horizontal obstruction of the vegetation for flowing water, whereas laser point height distribution is a function of detectability in the direction of the laser pulses, which is primarily vertical. With all plots included, straightforward application of the equations for Percentage Index and the Vegetation Area Index (Equations 1 and 2) to the laser data yielded no improvement over the traditional method based on ecotope mapping, which does not take variability within ecotopes into account. Compared to other laser scanning studies, these results explain little regarding the field variance, as other papers reported variances between 42 and 96 percent (Nilsson, 1996; Næsset, 1997; Means *et al.*, 1999; Lefsky *et al.*, 1999a; Lefsky *et al.*, 1999b; Næsset and Bjerknes, 2001; Næsset, 2002; Drake *et al.*, 2002; Asselman, 2002).

The first reason for the low predictive quality of the initial regression models was that the minimum number of points in the interval between  $h1$  and  $h2$  was not reached for many field plots. Therefore, the simulation was used to decide upon the minimum number of points needed, which appeared to be 50, which improved the results of the laser-derived methods significantly ( $R^2$  was 0.55 for  $PI_{valid}$  and 0.33 for  $VAI_{valid}$  based on valid points only). The reason for so few laser hits in the inundation height interval can result from a very dense crown layer, from absorption of laser energy by the vegetation, combined with a too small plot size.

The second problem that resulted in low predictive quality was the loss of returns. Lefsky *et al.* (1999a) also addressed the issue of different reflectivity between ground and vegetation surfaces, and simply compensated by multiplying the ground returns by two. However, this does not consider spatial variability in reflectivity. Many more invalid points were present in the DW-ADW dataset than in the GW dataset. The reorientation of the scanner between 2001 and 2003 led to a greater chance of mirroring away of laser energy on a horizontal target, as higher incidence angles result from the reorientation. Therefore, it can not be the cause of the lower number of invalid points for the gw dataset. An indication for this difference can be found in the differences in reflection intensities between the two datasets, which also was significantly higher for gw. This indicates that more energy was available due to a newer laser, which improves detection of the returned laser pulse. Reconstructing the position of the invalid points showed unexpected results. The first assumption was that all points got absorbed at the ground surface (Figure 8a and Figure 9c and 9d).

However, by assigning the ground height to the invalid point, the reference plots from the CW data set show up as large outliers in the scatter plot ( $VAI_{inv,grd}$  in Figure 9d,  $R^2 = 0.27$ ). Due to the large number of invalid points, the  $VAI$  values for DW-ADW were underestimated when compared to plots in the Gamenen floodplain with few invalid points. This indicates that absorption of the laser energy indeed did not occur only at the ground surface. The second assumption was, therefore, that only points with a high point density ratio were absorbed at the ground surface, while the other points were excluded from the analysis. This results in higher  $VAI$  values ( $VAI_{inv,PDR}$  in Figure 9f,  $R^2 = 0.36$ ) as fewer points are assigned to the ground surface. However, the CW plots still shows up as outliers in the scatter plot, reducing the overall explained variance. The Percentage Index, after reassigning coordinates of the invalid points using the point density ratio, appeared the better predictor of hydrodynamic vegetation density ( $R^2 = 0.66$ , Figure 9e), which is valid for deciduous forests with understorey under leaf-off conditions. Although this parameter does not take occlusion from the crown area into account, it is less sensitive to the uncertainty in the number of ground points (Figure 7c), resulting in the best overall prediction. Compared to the ecotope approach this is a major improvement as the residual standard error (RSE) drops by 33 percent. Portability of the method remains to be assessed, but the relation will not hold for forests with a closed canopy, such as pine, as the  $PI$  does not take occlusion into account. Shrubs have a higher detectability for laser pulses as their stems grow more horizontally, and the established relation will probably overestimate shrub density.

A third source of unexplained variance is the positional error of the field reference plots, resulting from the use of a handheld GPS, with manual correction made using the ecotope maps. The forests showed spatial variation in vegetation density, and the field reference density might therefore refer to an area that not fully overlaps with laser-derived  $VAI$ . A final source of error is the assumption of cylindrical vegetation elements of the forest, and that field measurements are taken at breast height, whereas the laser data represents the interval between 0.5 m and 2.5 m above the forest floor. More accurate field measurements could be made using photographic techniques (e.g., Zehm *et al.*, 2003; Jonckheere *et al.*, 2004).

The simulation study showed that the incidence angle potentially has a large effect on both  $PI$  and  $VAI$  (Figure 7b). The effect on  $PI$  and  $VAI$  of the field plots is potentially large because the size of the field plots was approximately 20 by 20 meters. Therefore, the plots were too small to cover the full width of a scan strip, limiting the range of incidence angles within a single plot. Holmgren *et al.* (2003) found in their simulation study that scan angle had a significant effect on laser quantile heights of the canopy of pine and spruce forests. A larger effect was found in forests with a low tree density. The effect of the incidence angle, however, was not confirmed by the field data in this study. Plot-averaged incidence angles varied between 10° and 23°, but adding the incidence angle as a predictor to the multiple regressions did not significantly improve the results. This could be solved by constructing a more realistic model of leafless trees (e.g., Kay and Kajiya, 1986). To make airborne laser scanners more suitable for vegetation density mapping, the laser scanner hardware and software should focus on improved detection of vertical stems. Scan angles should therefore be increased by tilting the laser scanner to a more oblique direction, while remaining within the maximum range of the scanner (Skaloud *et al.*, 2005). Additionally, waveform digitizing laser scanning might solve the problem of detecting low

energy returns from forests, since it does not use a threshold (Wagner *et al.*, 2004).

## Conclusions

This paper describes the extraction of hydrodynamic vegetation density from airborne laser scanning data, which can be used for hydrodynamic models that assume rigid vegetation. Two different models to predict vegetation density were tested and compared to the traditional approach, in which manually delineated plots are labeled using a lookup table: (a) Percentage Index ( $PI$ ), which considers the relative number of points in the inundation height interval, and (b) the Vegetation Area Index ( $VAI$ ) based on the method of MacArthur and Horn (1969). Both predictors have the advantage that they consider the interval inundated by the water during peak discharges of the river, contrary to any spectral remote sensing method. Both methods relate the vertical point distribution of the laser point cloud to hydrodynamic vegetation density. A minimum of 50 laser points should be included in the laser-estimate to avoid large errors from random sampling of trees. In a novel approach, the emitted laser pulses that did not generate a significant return were included in the data processing as well. Assessment of the number of invalid points is an important check for any laser-based regression model that uses percentiles, as percentile height will shift with the number of invalid points. Subsequent reconstruction of the location where the energy got absorbed enabled the incorporation of these points into the computation of  $PI$  and  $VAI$ . The Percentage Index, with the invalid points reconstructed by means of thresholding the point density ratio, is the best predictor ( $R^2 = 0.66$ ,  $RSE = 0.018 \text{ m}^{-1}$ ) of vegetation density of deciduous floodplain forests including undergrowth under leaf-off condition. This relationship is not valid for pine forests and shrubs. The Percentage Index is an improvement over the current ecotope approach ( $R^2 = 0.28$ ,  $RSE = 0.024 \text{ m}^{-1}$ ). Moreover, this method can be applied to map 2D spatial patterns in vegetation density within floodplain forest, which includes an estimate of the prediction error. Both were previously unavailable.

Computer simulation of  $VAI$  and  $PI$  based on synthetic data showed that:

- $VAI$  increases linearly with vegetation density, while  $PI$  initially increases and then decreases with increasing vegetation density.
- A minimum number of 50 points in the height interval under considerations per estimate is needed for accurate computation of  $PI$  and  $VAI$ .
- $PI$  and  $VAI$  increase with higher incidence angles of the laser pulses.
- $VAI$  has a stronger dependence on non-returned ground points than  $PI$ .

To improve vegetation density mapping using airborne laser scanning, the recommendation is to:

- Increase the size of forest field plots for dense canopies to meet the requirement of a minimum number of points in the height interval of interest.
- Use field methods that have a larger physical sampling size and do not need the assumption of cylindrical vegetation.
- Increase the energy of the laser scanner to as much as is legally allowed to limit loss of laser hits on vegetation.
- Change the viewing angle of one of the laser scanners to the maximum forward direction, for example 45°, to increase the detection of vertical stems.
- Investigate in last instance the relation between vegetation density and other parameters such as laser-derived vegetation height, or individual trees, which will have to solve the problem of relating tree crown properties to the vegetation density in the inundation height.

## Acknowledgments

This work was funded by NWO, the Netherlands Organization for Scientific Research, within the framework of the LOICZ program under Contract Number 01427004. I thank the AGI, the Advisory Board on Geo-informatics and ICT of the Dutch Ministry of Transport, Public Works and Water Management for providing the laser scanner datasets. Luc Amoureux of Fugro-Inpark is "in the name of science" gratefully acknowledged for exporting the laser scan data again in its final raw data form.

## References

- Aber, J.D., 1979. A method for estimating foliage-height profiles in broad leaved forests, *Journal of Ecology*, 67:35–40.
- Asselman, N.E.M., 2002. *Laser Altimetry and Hydraulic Roughness of Vegetation, Further Studies Using Ground Truth*, Delft Hydraulics, Q3139:WL, Delft.
- Baltsavias, E.P., 1999a. Airborne laser scanning: basic relations and formulas, *ISPRS Journal of Photogrammetry and Remote Sensing*, 54:199–214.
- Baltsavias, E.P., 1999b. Airborne laser scanning: Exciting systems and firms and other resources, *ISPRS Journal of Photogrammetry and Remote Sensing*, 64:164–198.
- Baptist, M.J., V. Babovich, J. Rodríguez-Uthurburu, M. Keijzer, R.E. Uittenbogaard, A. Mynett, and A. Verwey, 2007. On inducing equations for vegetation resistance, *Journal of Hydraulic Research*, 45(4).
- Brown, J.K., 1971. A planar intersect method for sampling fuel volume and surface area, *Forest Science*, 17:96–102.
- Cobby, D.M., D.C. Mason, and I.J. Davenport, 2001. Image processing of airborne scanning laser altimetry data for improved river flood modeling, *ISPRS Journal of Photogrammetry and Remote Sensing*, 56(2):121–138.
- Cobby, D.M., D.C. Mason, M.S. Horrit and P.D. Bates, 2003. Two-dimensional hydraulic flood modelling using a finite-element mesh decomposed according to vegetation and topographic features derived from airborne scanning laser altimetry, *Hydrological Processes*, 17:1979–2000.
- Copeland, R.R., 2000. *Determination of Flow Resistance Coefficients Due to Shrubs and Woody Vegetation*, ERDC/CHL CHETN-VIII-3, U.S. Army Corps of Engineers
- Cusack, G.A., M.F. Hutchinson, and J.D. Kalma, 1999. Calibrating airborne vegetation data for hydrological applications under dry conditions, *International Journal of Remote Sensing*, 20(11):2221–2233.
- Darby, S.E., 1999. Effect of riparian vegetation on resistance and flood potential, *Journal of Hydraulic Engineering*, 125:443–454.
- Davenport, I.J., R.B. Bradbury, G.R.F. Anderson, J.R. Hayman, J.R. Krebs, D.C. Mason, J.D. Wilson, and N.J. Veck, 2000. Improving bird population models using airborne remote sensing, *International Journal of Remote Sensing*, 21:2705–2717.
- Den Ouden, J.B., 1993. *Het Aangestroomd Oppervlak van Geïnnundeerde Ooibossen in Diverse Ontwikkelingsstadia*, IBN-Rapport 039, IBN-DLO, Wageningen (in Dutch).
- Drake, J.B., R.O. Dubayah, D.B. Clark, R.G. Knox, J.B. Blair, M.A. Hofton, R.L. Chazdon, J.F. Weishampel, and S. Prince, 2002. Estimation of tropical forest structural characteristics using large-footprint lidar, *Remote Sensing of Environment*, 79:305–319.
- Helmiö, T., 2002. Unsteady 1D flow model of compound channel with vegetated floodplains, *Journal of Hydrology*, 269:89–99.
- Holmgren, J., and T. Jonsson, 2004. Large scale airborne laser scanning of forest resources in Sweden, *Laser-Scanners for Forest and Landscape Assessment* (M. Thies, B. Koch, H. Spiecker, and H. Weinackers, editors), Institute for Forest Growth, Freiburg, Germany, unpaginated CD-ROM.
- Holmgren, J., M. Nilsson, and H. Olsson, 2003. Simulating the effect of lidar scanning angle of mean tree height and canopy closure, *Canadian Journal of Remote Sensing*, 29:623–632.
- Hopkinson, C., L.E. Chasmer, G. Sass, I.F. Creed, M. Sitar, W. Kalbfleisch, and P. Treitz, 2005. Vegetation class dependent errors in lidar ground elevation and canopy height estimates in a boreal wetland environment, *Canadian Journal of Forest Research*, 31:191–206.
- Huisling, E.J., and L.M. Gomes-Pereira, 1998. Errors and accuracy estimates of laser data acquired by various laser scanning systems for topographic applications, *ISPRS Journal of Photogrammetry and Remote Sensing*, 53:245–261.
- Huthoff, F., and D. Augustijn, 2004. Sensitivity analysis of flood-plain roughness in 1D flow, *Proceedings of the 6<sup>th</sup> International Conference on Hydroinformatics* (S.Y. Liong, S.I. Phoon, and V. Babovichs, editors), Singapore, Malaysia, pp. 301–308.
- Jansen, B.J.M., and J.J.G.M. Backx, 1998. *Ecotope Mapping Rhine Branches-East 1997*, 98.054, RIZA, Lelystad (in Dutch).
- Jonckheere, I., S. Fleck, K. Nackaerts, B. Muys, P. Coppin, M. Weiss, and F. Baret, 2004. Review of methods for in situ leaf area index determination: Part I. Theories, sensors and hemispherical photography, *Agricultural and Forest Meteorology*, 121:19–35.
- Kay, T.L., and J.T. Kajiya, 1986. Ray tracing complex scenes, *Computer Graphics*, 20:269–278.
- Klaassen, G.J., C. Stolker, E.H. Van Velzen, and H. Verhey, 1999. *Naar een Ruwheidsvoorspeller voor Moerasvegetatie op Basis van Riet en Gras*, RIZA Werkdocument 2000.166X, Delft Hydraulics, RIZA, Delft, Arnhem (in Dutch).
- Klopstra, D., H. Barneveld, J.M. Van Noortwijk, and E.H. Van Velzen, 1997. Analytical model for hydraulic roughness of submerged vegetation, *Proceedings of the 27<sup>th</sup> International IAHR Conference*, San Francisco, pp. 775–780.
- Kouwen, N., and M. Fathi-Moghadam, 2000. Friction factors for coniferous trees along rivers, *Journal of Hydraulic Engineering*, 126:732–740.
- Kraus, K., and N. Pfeifer, 1998. Determination of terrain models in wooded areas with airborne laser scanner data, *ISPRS Journal of Photogrammetry and Remote Sensing*, 53:193–203.
- Lefsky, M.A., W.B. Cohen, S.A. Acker, G.G. Parker, T.A. Spies, and D. Harding, 1999a. Lidar remote sensing of the canopy structure and biophysical properties of Douglas-fir western hemlock forests, *Remote Sensing of Environment*, 70:339–361.
- Lefsky, M.A., D. Harding, W.B. Cohen, G. Parker, and H.H. Shugart, 1999b. Surface lidar remote sensing of basal area and biomass in deciduous forests of eastern Maryland, USA, *Remote Sensing of Environment*, 67:83–98.
- Leuven, R.S.E.W., Y. Gerig, I. Poudevigne, G.W. Geerling, L. Kooistra, and B.G.W. Aarts, 2002. Cumulative impact assessment of ecological rehabilitation and infrastructure facilities in flood-plains along the middle reach of the River Waal, *Application of Geographic Information Systems and Remote Sensing in River Studies* (R.S.E.W. Leuven, I. Poudevigne, and R.M. Teeuw, editors), Backhuys Publishers, Leiden, pp. 247.
- MacArthur, R.H., and H.S. Horn, 1969. Foliage profile by vertical measurements, *Ecology*, 50.
- Mason, D.C., D.M. Cobby, M.S. Horrit, and P. Bates, 2003. Flood-plain friction parameterization in two-dimensional river food models using vegetation heights derived from airborne scanning laser altimetry, *Hydrological Processes*, 17:1711–1732.
- Means, J.E., S.A. Acker, D.J. Harding, J.B. Blair, M.A. Lefsky, W.B. Cohen, M.E. Harmon, and W.A. McKee, 1999. Use of large-footprint scanning airborne lidar to estimate forest stand characteristics in the western Cascades of Oregon, *Remote Sensing of Environment*, 67:298–308.
- Mertens, W., 1989. Zur frage hydraulischer berechnungen naturnaher fließgewässer, *Wasserwirtschaft*, 79:170–179 (in German).
- Mertes, L.A.K., 2002. Remote sensing of riverine landscapes, *Freshwater Biology*, 47:799–816.
- Mertes, L.A.K., D.L. Daniel, J.M. Melack, B. Nelson, L.A. Martinelli, and B.R. Forsberg, 1995. Spatial patterns of hydrology, geomorphology, and vegetation on the floodplain of the Amazon River in Brazil from a remote sensing perspective, *Geomorphology*, 13:215–232.
- Naesset, E., 1997. Geographical information systems in long-term forest management and planning with special reference to preservation of biological diversity: A review, *Forest Ecology and Management*, 93:121–136.

- Naasset, E., 2002. Predicting forest stand characteristics with airborne scanning laser using a practical two-stage procedure and field data, *Remote Sensing of Environment*, 80:88–99.
- Naasset, E., and K.-O. Bjercknes, 2001. Estimating tree heights and number of stems in young forest stands using airborne laser scanner data, *Remote Sensing of Environment*, 78:328–340.
- Nienhuis, P.H., and R.S.E.W. Leuven, 2001. River restoration and flood protection: Controversy or synergism?, *Hydrobiologia*, 444:85–99.
- Nilsson, M., 1996. Estimating tree heights and stand volume using an airborne lidar system, *Remote Sensing of Environment*, 56:1–7.
- Pasche, E., 1984. *Turbulenzmechanismen in naturnahen Fließgewässern und die Möglichkeit ihrer Mathematischen Erfassung*, Mitteilung des Instituts für Wasserbau, 52 TWTH, Aachen.
- Petryk, S., and G. Bosmajian, 1975. Analysis of flow through vegetation, *Journal of Hydraulics Divisions*, 101:871–884.
- Ringrose, S., W. Matheson, and T. Boyle, 1988. Differentiation of ecological zones in the Okavango delta, Botswana by classification and contextual analyses of Landsat MSS data, *Photogrammetric Engineering & Remote Sensing*, 54(6):601–608.
- Ritzen, M.R., and M.W. Straatsma, 2002. *Laseraltimetrie en Hydraulische Vegetatie Ruwheid van Uiterwaarden*, NCR-Publicatie, 19–2002, Delft.
- Schröder, W., and A. Nuding, 1986. Spiegellinienberechnung für einen wildbach mit Gehölzufern, *Wasserwirtschaft*, 76 (in German).
- Skaloud, J., J. Vallet, K. Keller, G. Vessière, and O. Kölbl, 2005. Helimap: Rapid large scale mapping using handheld LiDAR/CCD/GPS/INS sensors on helicopters, *Proceedings of the ION GNSS Congress*, Long Beach, California.
- Stolker, C., E.H. Van Velzen, and G.J. Klaassen, 1999. *Nauwkerigheidanalyse Stromingsweerstand Vegetatie*, 99.192x, Delft Hydraulics, RIZA, Delft, Arnhem (in Dutch).
- Straatsma, M.W., and H. Middelkoop, 2006. Airborne laser scanning as a tool for lowland floodplain vegetation monitoring, *Hydrobiologia*, 565:87–103.
- Townsend, P.A., and J. Walsh, 2001. Remote sensing of forested wetlands: Application of multitemporal and multispectral satellite imagery to determine plant community composition and structure in southeastern USA, *Plant Ecology*, 157:129–149.
- Tsujimoto, T., 1999. Fluvial processes in streams with vegetation, *Journal of Hydraulic Engineering*, 37:789–803.
- Van der Sande, C.J., S.M. De Jong, and A.P.J. De Roo, 2003. A segmentation and classification approach of IKONOS-2 imagery for land cover mapping to assist flood risk and flood damage assessment, *International Journal of Applied Earth Observation and Geoinformation*, 4:217–229.
- Van Stokkom, H.T.C., A.J.M. Smits, and R.S.E.W. Leuven, 2005. Flood defense in the Netherlands: A new era, a new approach, *Water International*, 30:76–87.
- Van Velzen, E.H., P. Jesse, P. Cornelissen, and H. Coops, 2003. *Stromingsweerstand Vegetatie in Uiterwaarden*, 2003.028, RIZA, Arnhem (in Dutch).
- Wagner, W., A. Ulrich, T. Melzer, C. Brieke, and K. Kraus, 2004. From single pulse to full waveform digitizing laser scanners: Potential and practical challenges, *Proceedings of the XX ISPRS Congress*, Istanbul, Turkey.
- Wehr, A., and U. Lohr, 1999. Airborne laser scanning – An introduction and overview, *ISPRS Journal of Photogrammetry and Remote Sensing*, 54:68–82.
- Zehm, A., M. Nobis, and A. Schwabe, 2003. Multiparameter analysis of vertical vegetation structure based on digital image processing, *Flora*, 198:142–160.

(Received 10 October 2006; accepted 13 November 2006; revised 06 December 2006)